Boundary layer structure in turbulent thermal convection and its consequences for the required numerical resolution

2010 New J. Phys. 12 075022

(http://iopscience.iop.org/1367-2630/12/7/075022)

New Journal of Physics
The open-access journal for physics

Boundary layer structure in turbulent thermal convection and its consequences for the required numerical resolution

Olga Shishkina[1,4], Richard J A M Stevens[2], Siegfried Grossmann[3] and Detlef Lohse[2]

[1] DLR—Institute for Aerodynamics and Flow Technology, Bunsenstraße 10, D-37073 Göttingen, Germany
[2] Department of Science and Technology, Impact Institute and J M Burgers Center for Fluid Dynamics, University of Twente, PO Box 217, 7500 AE Enschede, The Netherlands
[3] Fachbereich Physik der Philipps-Universität, Renthof 6, D-35032 Marburg, Germany
E-mail: Olga.Shishkina@dlr.de, R.J.A.M.Stevens@tnw.utwente.nl, d.lohse@utwente.nl and grossmann@physik.uni-marburg.de

New Journal of Physics **12** (2010) 075022 (17pp)
Received 2 May 2010
Published 26 July 2010
Online at http://www.njp.org/
doi:10.1088/1367-2630/12/7/075022

Abstract. Results on the Prandtl–Blasius-type kinetic and thermal boundary layer (BL) thicknesses in turbulent Rayleigh–Bénard (RB) convection in a broad range of Prandtl numbers are presented. By solving the laminar Prandtl–Blasius BL equations, we calculate the ratio between the thermal and kinetic BL thicknesses, which depends on the Prandtl number $\mathcal{P}r$ only. It is approximated as $0.588\mathcal{P}r^{-1/2}$ for $\mathcal{P}r \ll \mathcal{P}r^*$ and as $0.982\mathcal{P}r^{-1/3}$ for $\mathcal{P}r^* \ll \mathcal{P}r$, with $\mathcal{P}r^* \equiv 0.046$. Comparison of the Prandtl–Blasius velocity BL thickness with that evaluated in the direct numerical simulations by Stevens *et al* (2010 *J. Fluid Mech.* **643** 495) shows very good agreement between them. Based on the Prandtl–Blasius-type considerations, we derive a lower-bound estimate for the minimum number of computational mesh nodes required to conduct accurate numerical simulations of moderately high (BL-dominated) turbulent RB convection, in the thermal and kinetic BLs close to the bottom and top plates. It is shown that the number of required nodes within each BL depends on $\mathcal{N}u$ and $\mathcal{P}r$ and grows with the Rayleigh number $\mathcal{R}a$ not slower than $\sim\mathcal{R}a^{0.15}$. This estimate is in excellent

[4] Author to whom any correspondence should be addressed.

agreement with empirical results, which were based on the convergence of the Nusselt number in numerical simulations.

Contents

1. Introduction

Rayleigh–Bénard (RB) convection is the classical system for studying the properties of thermal convection. In this system, a layer of fluid confined between two horizontal plates is heated from below and cooled from above. Thermally driven flows are of utmost importance in industrial applications and in natural phenomena. Examples include the thermal convection in the atmosphere, the ocean, in buildings, in process technology and in metal-production processes. In the geophysical and astrophysical context, one may think of convection in the Earth's mantle, in the Earth's outer core and in the outer layer of the Sun. For example, the random reversals of the Earth's or the Sun's magnetic field have been connected with thermal convection.

Major progress in the understanding of the RB system has been made over recent decades, see e.g. the recent reviews [1, 2]. Meanwhile, it has been well established that the general heat transfer properties of the system, i.e. $\mathcal{N}u = \mathcal{N}u(\mathcal{R}a, \mathcal{P}r)$ and $\mathcal{R}e = \mathcal{R}e(\mathcal{N}u, \mathcal{P}r)$, are well described by the Grossmann–Lohse (GL) theory [3]–[6]. In that theory, in order to estimate the thicknesses of the kinetic and thermal boundary layers (BLs) and the viscous and thermal dissipation rates, the BL flow is considered to be scalingwise laminar Prandtl–Blasius flow over a plate. We use the conventional definitions: the Rayleigh number is $\mathcal{R}a = \alpha g H^3 \Delta/\nu\kappa$ with the isobaric thermal expansion coefficient α, the gravitational acceleration g, the height H of the RB system, the temperature difference Δ between the heated lower plate and the cooled upper plate, and the material constants ν (kinematic viscosity) and κ (thermal diffusivity), both considered to be constant in the container (Oberbeck–Boussinesq approximation). The Prandtl number is defined as $\mathcal{P}r = \nu/\kappa$ and the Reynolds number $\mathcal{R}e = UH/\nu$, with the wind amplitude U that forms in the bulk of the RB container.

The assumption of a laminar BL will break down if the shear Reynolds number $\mathcal{R}e_s$ in the BLs becomes larger than approximately 420 [7]. Most experiments and direct numerical simulations (DNS) currently available are in regimes where the BLs are expected to be still (scalingwise) laminar: see [1]. Indeed, experiments have confirmed that the BLs scalingwise behave as in laminar flow [8], i.e. follow the *scaling predictions* of the Prandtl–Blasius

theory [7], [9]–[13]. Recently, Zhou *et al* [14, 15] have shown that not only the scaling of the thickness but also the experimental and numerical *BL profiles* in RB convection agree perfectly with the Prandtl–Blasius profiles if they are evaluated in the time-dependent reference frames, based on the respective *momentary* thicknesses. This confirms that the Prandtl–Blasius BL theory is indeed the relevant theory to describe the BL dynamics in RB convection for not too large $\mathcal{R}e_s$.

The aim of this paper is to explore the consequences of the Prandtl–Blasius theory for the required numerical grid resolution of the BLs in DNSs. Hitherto, convergence checks could only be done *a posteriori*, by checking whether the Nusselt number does not change considerably with increasing grid resolution [16]–[21] or by guaranteeing (e.g. in [21, 22]) that the Nusselt numbers calculated from the global energy dissipation rate or thermal dissipation rate agree well with those calculated from the temperature gradient at the plates or those obtained from the overall heat flux. The knowledge that the profiles are of Prandtl–Blasius type offers the opportunity to *a priori* determine the number of required grid points in the BLs for a given Rayleigh number and Prandtl number, valid in the BL-dominated ranges of moderately high $\mathcal{R}a$ numbers.

In section 2, we will first revisit the Prandtl–Blasius BL theory—see [7], [9]–[13] or, for more recent discussions in the context of RB, [6, 23]—and derive the ratio between the thermal BL thickness δ_θ and the velocity BL thickness δ_u as functions of the Prandtl number $\mathcal{P}r$ extending previous work (section 3). We will also discuss the limiting cases for large and small $\mathcal{P}r$, respectively. The transitional Prandtl number between the two limiting regimes turns out to be surprisingly small, namely $\mathcal{P}r^* = 0.046$. The crossover range is found to be rather broad, roughly four orders of magnitude in $\mathcal{P}r$. In section 4, we note that the Prandtl–Blasius velocity BL thickness is different from the velocity BL thickness based on the position of the maximum rms velocity fluctuations (widely used in the literature), but agrees well with a BL thickness based on the position of the maximum of an energy dissipation derivate that was recently introduced in [21, 24]. We then derive the estimate for the minimum number of grid points that should be placed in the BLs close to the top and bottom plates, in order to guarantee proper grid resolution. Remarkably, the number of grid points that must have a distance smaller than δ_u from the wall *increases* with increasing $\mathcal{R}a$, roughly as $\sim\mathcal{R}a^{0.15}$. This estimate was compared with *a posteriori* results for the required grid resolution obtained in various DNSs of the last three decades, and good agreement was found. Section 5 is devoted to conclusions.

2. Prandtl BL equations

The Prandtl–Blasius BL equations for the velocity field $\mathbf{u}(x, z)$ (assumed to be two-dimensional (2D) and stationary) over a semi-infinite horizontal plate [7], [9]–[13] read

$$u_x \partial_x u_x + u_z \partial_z u_x = \nu \partial_z \partial_z u_x, \tag{1}$$

with the boundary conditions $u_x(x, 0) = 0$, $u_z(x, 0) = 0$ and $u_x(x, \infty) = U$. Here, $u_x(x, z)$ is the horizontal component of the velocity (in the direction x of the large-scale circulation), $u_z(x, z)$ the vertical component of the velocity (in the direction z perpendicular to the plate) and U the horizontal velocity outside the kinetic BL (wind of turbulence). Correspondingly, the equation determining the (stationary) temperature field $T(x, z)$ reads

$$u_x \partial_x T + u_z \partial_z T = \kappa \partial_z \partial_z T, \tag{2}$$

with the boundary conditions $T(x,0) = T_{\rm plate}$ and $T(x,\infty) = T_{\rm bulk}$, which under the Oberbeck–Boussinesq conditions is the arithmetic mean of the upper and lower plate temperatures. Applying these equations to RB flow implies that we assume the temperature field to be passive.

The dimensionless similarity variable ξ for the vertical distance z from the plate measured at distance x from the plate's edge is

$$\xi = z\sqrt{\frac{U}{x\nu}}. \tag{3}$$

Since the flow in Prandtl theory is 2D, a streamfunction $\hat{\Psi}$ can be introduced, which represents the velocity field. The streamfunction is non-dimensionalized as $\Psi = \hat{\Psi}/\sqrt{x\nu U}$, and the temperature is measured in terms of $\Delta/2$, giving the non-dimensional temperature field Θ. Rewriting equations (1) and (2) in terms of Ψ and Θ, one obtains

$$\mathrm{d}^3\Psi/\mathrm{d}\xi^3 + 0.5\Psi\,\mathrm{d}^2\Psi/\mathrm{d}\xi^2 = 0, \tag{4}$$

$$\mathrm{d}^2\Theta/\mathrm{d}\xi^2 + 0.5\mathcal{P}r\,\Psi\,\mathrm{d}\Theta/\mathrm{d}\xi = 0. \tag{5}$$

Here the boundary conditions are

$$\Psi(0) = 0, \quad \mathrm{d}\Psi/\mathrm{d}\xi(0) = 0, \quad \mathrm{d}\Psi/\mathrm{d}\xi(\infty) = 1, \tag{6}$$

$$\Theta(0) = 0, \quad \Theta(\infty) = 1. \tag{7}$$

The temperature and velocity profiles obtained from numerically solving equations (4)–(7) (for particular Prandtl numbers) are already shown in textbooks [7, 12, 13] and in the context of RB convection in [23, 25]: from the momentum equation (6) with the above boundary conditions, one immediately obtains the horizontal velocity $\mathrm{d}\Psi/\mathrm{d}\xi$. The dimensionless kinetic BL thickness $\tilde{\delta}_u$ can be defined as that distance from the plate at which the tangent to the function $\mathrm{d}\Psi/\mathrm{d}\xi$ at the plate ($\xi = 0$) intersects the straight line $\mathrm{d}\Psi/\mathrm{d}\xi = 1$ (see figure 1(a)). As equation (4) and the boundary conditions (6) contain no parameter whatsoever, the *dimensionless* thickness $\tilde{\delta}_u$ of the kinetic BL with respect to the similarity variable ξ is universal, i.e. independent of $\mathcal{P}r$ and U or $\mathcal{R}e$,

$$\tilde{\delta}_u = A^{-1} \approx 3.012 \quad \text{or} \quad A \approx 0.332. \tag{8}$$

Solving numerically equation (5) with the boundary conditions (7) for any fixed Prandtl number, one obtains the temperature profile with respect to the similarity variable ξ (see figure 1(b)). Note that, in contrast to the longitudinal velocity $\mathrm{d}\Psi/\mathrm{d}\xi$, the temperature profile Θ depends not only on ξ but also on the Prandtl number, since $\mathcal{P}r$ appears in equation (5) as the (only) parameter. The distance from the plate at which the tangent to the Θ profile intersects the straight line $\Theta = 1$ defines the dimensionless thickness of the thermal BL,

$$\tilde{\delta}_\theta = C(\mathcal{P}r), \tag{9}$$

where $C(\mathcal{P}r)$ is a certain function of the Prandtl number. For example, one numerically finds $C \approx 3.417$, 1.814 and 1.596 for $\mathcal{P}r = 0.7$, 4.38 and 6.4, respectively (see figure 1(b)).

From (8) and (9), one obtains the ratio between the (dimensional) thermal BL thickness δ_θ and the (dimensional) kinetic BL thickness δ_u:

$$\frac{\delta_\theta}{\delta_u} = \frac{\tilde{\delta}_\theta}{\tilde{\delta}_u} = AC(\mathcal{P}r). \tag{10}$$

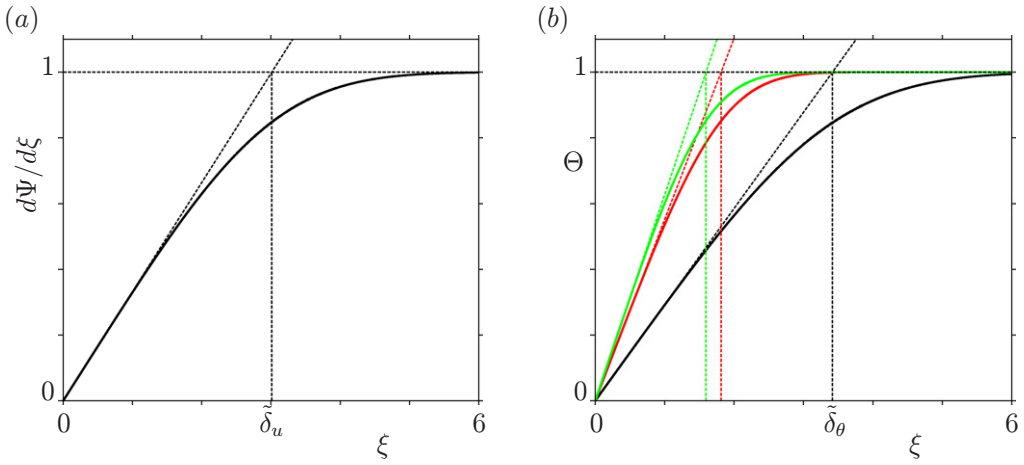

Figure 1. Solution of the Prandtl–Blasius equations (4)–(7): (a) longitudinal velocity profile $d\Psi/d\xi(\xi)$ (solid curve) with respect to the similarity variable ξ. The tangent to the longitudinal velocity profile at the plate ($\xi = 0$) and the straight line $d\Psi/d\xi = 1$ (both dashed lines) intersect at $\xi = \tilde{\delta}_u \equiv A^{-1} \approx 3.012$, for all $\mathcal{P}r$. We define this value $\tilde{\delta}_u$ as the thickness of the kinetic BL. (b) Temperature profile $\Theta(\xi)$ as a function of the similarity variable ξ for $\mathcal{P}r = 0.7$ (black solid curve), $\mathcal{P}r = 4.38$ (red solid curve) and $\mathcal{P}r = 6.4$ (green solid curve). The tangents to the profile curves at the plate ($\xi = 0$) and the straight line $\Theta = 1$ (dashed lines) define the edges (thicknesses) of the corresponding thermal BLs, i.e. $\xi = \tilde{\delta}_\theta \equiv C(\mathcal{P}r)$. For the presented cases $\mathcal{P}r = 0.7$, 4.38 and 6.4, one has $C(0.7) \approx 3.417$, $C(4.38) \approx 1.814$ and $C(6.4) \approx 1.596$, respectively.

As discussed above, the constant A and the function $C = C(\mathcal{P}r)$ are found from the solutions of equations (4)–(7) for different $\mathcal{P}r$. A and $C(\mathcal{P}r)$ reflect the slopes of the respective profiles:

$$A = \frac{d^2\Psi}{d\xi^2}(0), \quad C(\mathcal{P}r) = \left[\frac{d\Theta}{d\xi}(0)\right]^{-1}. \tag{11}$$

With (3) the physical thicknesses are $\delta_u = \tilde{\delta}_u/\sqrt{U/x\nu}$ and $\delta_\theta = \tilde{\delta}_\theta/\sqrt{U/x\nu}$, generally depending on U and the position x along the plate. The *physical* thermal BL thickness then is

$$\delta_\theta = \frac{C(\mathcal{P}r)}{\sqrt{U/(x\nu)}} = \left[\sqrt{\frac{U}{x\nu}}\frac{\partial\Theta}{\partial\xi}(0)\right]^{-1} = \left[\frac{\partial\Theta}{\partial z}(0)\right]^{-1}. \tag{12}$$

Thus, explicitly it depends either on U or on the position x along the plate. Recalling the definition of the thermal current $J = \langle u_z T\rangle - \kappa\partial_z\langle T\rangle$, we obtain $\langle\frac{\partial\Theta}{\partial z}(0)\rangle = \frac{1}{\Delta/2}\langle\frac{\partial T}{\partial z}(0)\rangle = \frac{2}{\kappa\Delta}J = 2H^{-1}\mathcal{N}u$, i.e. on x-average we have

$$\delta_\theta = \frac{H}{2\mathcal{N}u}. \tag{13}$$

δ_θ is the so-called slope thickness: see section 2.4 of [23]. In contrast to the thermal BL thickness δ_θ, the physical velocity BL thickness $\delta_u = A^{-1}/\sqrt{U/x\nu}$ depends explicitly both on the position x and on the wind amplitude U. In an RB cell, we choose for x a representative

value $x = \tilde{a}L = \tilde{a}\Gamma H$. Then the famous Prandtl formula [9] results:

$$\delta_u = \frac{aH}{\sqrt{\mathcal{R}e}}. \tag{14}$$

Here, $a = \sqrt{\tilde{a}\Gamma/A^2} = A^{-1}\sqrt{\tilde{a}\Gamma}$. The constant a has been obtained empirically [5], based on the experimental measurements of Qiu and Tong [26] performed in a cylindrical cell of aspect ratio one, filled with water. The result was the following [5]:

$$a \approx 0.482. \tag{15}$$

We note that this value probably depends on the aspect ratio and on the shape of the RB container and can also be different for numerical 2D RB convection [27]–[29]. It will also be different for the slope thickness as considered here or other definitions, e.g. the 99% thickness.

It seems worthwhile to note that similarly to the case of δ_θ, also δ_u can be expressed by a profile slope at the plate. Analogously to the temperature case, one calculates for the kinetic thickness $\delta_u = U/\frac{\partial u_x}{\partial z}(0)$. Here, U appears explicitly and the derivative may depend on $\mathbf{x}$. The denominator is the local stress tensor component, which—after averaging—describes the momentum transport, just as the temperature profile derivative at the plate characterizes the heat transport. In combination with equation (14), it means that the kinetic stress behaves as $\langle\frac{\partial u_x}{\partial z}(0)\rangle \sim U\sqrt{\mathcal{R}e}/(aH)$.

From equations (10) and (14) we also find the useful (and known) relation for the Prandtl–Blasius BLs:

$$\delta_\theta = a_\theta C(\mathcal{P}r)\frac{H}{\sqrt{\mathcal{R}e}} \quad \text{with } a_\theta = A \cdot a \approx 0.160. \tag{16}$$

From solving equations (4)–(7) together with relations (11), one finds that the BL thickness ratio (10) has two limiting cases, namely $\delta_\theta/\delta_u \sim \mathcal{P}r^{-1/2}$ for very small $\mathcal{P}r \ll 1$ and $\delta_\theta/\delta_u \sim \mathcal{P}r^{-1/3}$ for very large $\mathcal{P}r \gg 1$. We thus present the ratio of the thermal and kinetic BL thicknesses normalized by $\mathcal{P}r^{-1/3}$ in figure 2 for different $\mathcal{P}r$ from $\mathcal{P}r = 10^{-6}$–10^6. The figure confirms that the scaling of the ratio between the thermal and kinetic BL thicknesses in the low and high Prandtl number regimes is $\mathcal{P}r^{-1/2}$ and $\mathcal{P}r^{-1/3}$, respectively. Between these two limiting regimes, there is a transition region whose width is about four orders of magnitude in $\mathcal{P}r$. In the next section, we will derive analytic expressions for the ratio δ_θ/δ_u in the respective regimes, which will be used in the remainder of the paper to analyse the resolution properties for DNS in the BLs of the RB system.

In the Prandtl–Blasius theory the asymptotic velocity amplitude U is a given parameter; the resulting heat current $\mathcal{N}u$ is a performance of the BLs only. In contrast, in the RB convection the heat transport is determined by the BLs together with the bulk flow. Therefore in RB convection the wind amplitude U is no longer a passive parameter, but U and $\mathcal{N}u$ are actively coupled properties of the full thermal convection process.

The Reynolds number $\mathcal{R}e$ is defined as the dimensionless wind amplitude:

$$\mathcal{R}e = \frac{UH}{\nu}. \tag{17}$$

From the law for the kinetic BL thickness (14), the thermal BL thickness δ_θ (13) and the BL thickness ratio (10), one obtains

$$\mathcal{R}e = \left(\frac{aH}{\delta_u}\right)^2 = \left(\frac{\delta_\theta}{\delta_u}\right)^2\left(\frac{aH}{\delta_\theta}\right)^2 = 4a^2\mathcal{N}u^2\left(\frac{\delta_\theta}{\delta_u}\right)^2. \tag{18}$$

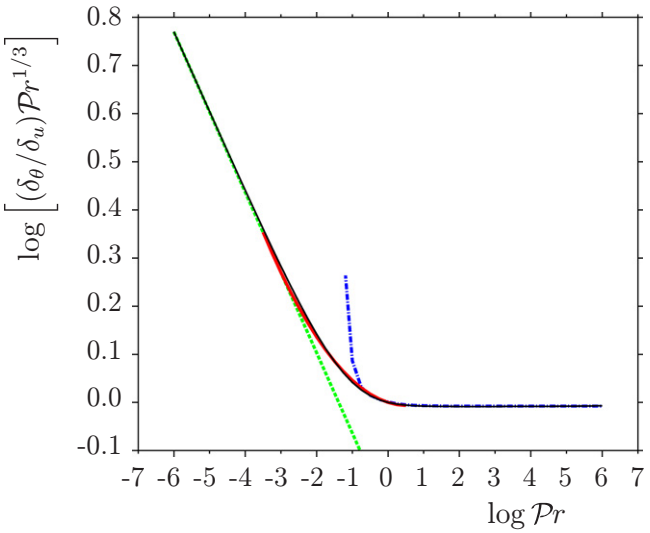

Figure 2. Double-logarithmic plot of the ratio between the thermal and kinetic BL thicknesses, normalized by $\mathcal{P}r^{-1/3}$, as obtained from numerical solution of equations (4)–(7) as a function of $\mathcal{P}r$ (solid black line). For large $\mathcal{P}r$ the curve through the data is constant; for small $\mathcal{P}r$ the (plotted, reduced) curve behaves $\propto \mathcal{P}r^{-1/6}$. Approximation (22) (green dotted line) is indistinguishable from δ_θ/δ_u in the region $\mathcal{P}r < 3 \times 10^{-4}$. Approximation (24) (blue dashed-dotted line) well represents δ_θ/δ_u for $\mathcal{P}r > 0.3$; for $\mathcal{P}r > 3$ it practically coincides with approximation (25). Approximation (26) (red solid curve) connects the analytical approximations in the transition range $3 \times 10^{-4} \leqslant \mathcal{P}r \leqslant 3$ between the lower and upper Prandtl number regimes.

This $\mathcal{R}e \sim \mathcal{N}u^2$ law is in perfect agreement with the GL theory [3]–[6]. In that theory, several sub-regimes in the $(\mathcal{R}a, \mathcal{P}r)$ parameter space are introduced, depending on the dominance of the BL or bulk contributions. In regimes I and II, the BL of the temperature field dominates, while in III and VI it is the thermal bulk. Regimes I and II differ in the velocity field contributions: it is either the u-BL (I) or the u-bulk (II) that dominates; analogously, the pair III and IV is characterized. The labels ℓ (for **l**ower $\mathcal{P}r$) and u (for **u**pper $\mathcal{P}r$) distinguish the cases in which the thermal BL is thicker or smaller than the kinetic one. All ranges in the GL theory, which are thermal BL dominated, show the $\mathcal{R}e \sim \mathcal{N}u^2$ behaviour, namely I_l, I_u, II_l, II_u. In the thermal bulk dominated ranges of RB convection, the relation between $\mathcal{R}e$ and $\mathcal{N}u$ is different. In III_u we have $\mathcal{R}e \sim \mathcal{N}u^{4/3}$, in IV_l it is $\mathcal{R}e \sim \mathcal{N}u$, and in IV_u also $\mathcal{R}e \sim \mathcal{N}u^{4/3}$ holds; but here the Prandtl–Blasius result (18) is not applicable, since the heat transport mainly depends on the heat transport properties of the bulk. In the range I_∞, although BL dominated, also a different relation ($\mathcal{R}e \sim \mathcal{N}u^3$) holds; here the upper and the lower kinetic BLs fill the whole volume and therefore there is no free flow outside the BLs, in contrast to the Prandtl–Blasius assumption of an asymptotic velocity with the LSC amplitude U.

3. Approximations for the ratio δ_θ/δ_u of the temperature and velocity BL thicknesses

In this section, we will derive analytical approximations for the ratio δ_θ/δ_u for the three regimes identified in the previous section (cf figure 2). We start by discussing the low ($\mathcal{P}r < 3 \times 10^{-4}$)

and high ($3 < \mathcal{P}r$) Prandtl number regimes, before we discuss the transition region $3 \times 10^{-4} \leqslant \mathcal{P}r \leqslant 3$.

3.1. Approximation of δ_θ/δ_u for $\mathcal{P}r < 3 \times 10^{-4}$

In the case of a very small Prandtl number, $\mathcal{P}r \ll 1$, the thickness of the velocity BL is negligible compared with the thickness of the temperature BL, i.e. $\delta_\theta \gg \delta_u$. Hence, in most of the thermal BL, it is $u_x \approx U$. Introducing the similarity variable as in [13],

$$\eta = \frac{z}{2}\sqrt{\frac{U}{x\kappa}}, \tag{19}$$

one obtains the following equation for the temperature as a function of η:

$$\mathrm{d}^2\Theta/\mathrm{d}\eta^2 + 2\eta\,\mathrm{d}\Theta/\mathrm{d}\eta = 0, \quad \text{with } \Theta(0) = 0, \quad \Theta(\infty) = 1.$$

The solution of this boundary value problem is the Gaussian error function:

$$\Theta(\eta) = \mathrm{erf}(\eta) \equiv \frac{2}{\sqrt{\pi}}\int_0^\eta \mathrm{e}^{-t^2}\,\mathrm{d}t. \tag{20}$$

According to (3) and (19), the similarity variable ξ used in the Prandtl equations and the similarity variable η used in the approximation for $\mathcal{P}r \ll 1$ are related as follows:

$$\eta = \tfrac{1}{2}\mathcal{P}r^{1/2}\xi. \tag{21}$$

Applying now formulae (20), (21) and (11), we obtain the following equalities:

$$\frac{2}{\sqrt{\pi}} = \frac{\mathrm{d}\Theta}{\mathrm{d}\eta}(0) = \frac{\mathrm{d}\Theta}{\mathrm{d}\xi}(0)\cdot\frac{\mathrm{d}\xi}{\mathrm{d}\eta} = \frac{1}{C(\mathcal{P}r)}\cdot 2\mathcal{P}r^{-1/2}.$$

This leads to the approximation for the function $C(\mathcal{P}r) = \sqrt{\pi}\mathcal{P}r^{-1/2}$ for very small $\mathcal{P}r$:

$$\frac{\delta_\theta}{\delta_u} = A\sqrt{\pi}\mathcal{P}r^{-1/2} \approx 0.588\mathcal{P}r^{-1/2}, \quad \mathcal{P}r \ll 1. \tag{22}$$

In figure 2, one can see that for very small Prandtl numbers, $\mathcal{P}r < 3 \times 10^{-4}$, approximation (22) is as expected indistinguishable from the numerically obtained δ_θ/δ_u.

3.2. Approximation of δ_θ/δ_u for $\mathcal{P}r > 3$

Meksyn [12], based on the work by Pohlhausen [11], derived that the solution of the temperature equation (5), together with relation (7), equals

$$\Theta\left(\frac{\xi}{\sqrt{2}}\right) = D\int_0^{\xi/\sqrt{2}} \mathrm{e}^{-F(t)\mathcal{P}r}\,\mathrm{d}t, \quad F(t) = \frac{1}{\sqrt{2}}\int_0^t \Psi(q)\mathrm{d}q. \tag{23}$$

The constant D can be found as usual from the boundary condition at infinity and was approximated in [11, 12] for $\mathcal{P}r > 1$ as follows:

$$D = \frac{0.478\mathcal{P}r^{1/3}}{c(\mathcal{P}r)}, \quad c(\mathcal{P}r) \approx 1 + \frac{1}{45\mathcal{P}r} - \frac{1}{405\mathcal{P}r^2} + \frac{161}{601425\mathcal{P}r^3} - \cdots.$$

From this and (23), one derives

$$\frac{0.478\mathcal{P}r^{1/3}}{c(\mathcal{P}r)} = D = \frac{\mathrm{d}\Theta}{\mathrm{d}(\xi/\sqrt{2})}(0) = \sqrt{2}\frac{\mathrm{d}\Theta}{\mathrm{d}\xi}(0) = \frac{\sqrt{2}}{C(\mathcal{P}r)}.$$

This connects $c(\mathcal{P}r)$ and $C(\mathcal{P}r)$, as follows:

$$C(\mathcal{P}r) \approx \frac{\sqrt{2}}{0.478}\, c(\mathcal{P}r)\mathcal{P}r^{-1/3} \approx 2.959\, c(\mathcal{P}r)\mathcal{P}r^{-1/3},$$

resulting in the approximation

$$\frac{\delta_\theta}{\delta_u} = AC(\mathcal{P}r) = E\mathcal{P}r^{-1/3}c(\mathcal{P}r), \quad E \approx A\frac{\sqrt{2}}{0.478} \approx 0.982. \tag{24}$$

For $\mathcal{P}r \gg 1$, the function $c(\mathcal{P}r)$ approaches 1, hence $C(\mathcal{P}r) \approx 2.959\mathcal{P}r^{-1/3}$, implying

$$\frac{\delta_\theta}{\delta_u} = E\mathcal{P}r^{-1/3}, \quad \mathcal{P}r \gg 1. \tag{25}$$

In figure 2, approximation (24) is presented as a blue dash-dotted curve. For $\mathcal{P}r > 3$, the function $(\delta_\theta/\delta_u)\mathcal{P}r^{1/3}$ almost coincides with the constant E.

3.3. Approximation of δ_θ/δ_u in the crossover range $3 \times 10^{-4} \leqslant \mathcal{P}r \leqslant 3$

As can be seen in figure 2, approximation (22) well represents δ_θ/δ_u in the region $\mathcal{P}r < 3 \times 10^{-4}$, while (25) is a good approximation of δ_θ/δ_u for $\mathcal{P}r > 3$. An approximation of the ratio between the thermal and kinetic BL thicknesses in the transition region $3 \times 10^{-4} \leqslant \mathcal{P}r \leqslant 3$ is obtained by applying a least square fit to the numerical solutions of the Prandtl–Blasius equations (4)–(7). One finds

$$\frac{\delta_\theta}{\delta_u} \approx \mathcal{P}r^{-0.357+0.022\log\mathcal{P}r}, \quad 3 \times 10^{-4} \leqslant \mathcal{P}r \leqslant 3. \tag{26}$$

As seen in figure 2, this relation is a good fit of the full solution in the transition regime.

3.4. Summary

For the ratio δ_θ/δ_u of the thicknesses of the thermal and kinetic BLs, which depends strongly (and only) on $\mathcal{P}r$, we find, according to (22), (25) and (26),

$$\frac{\delta_\theta}{\delta_u} = \begin{cases} A\sqrt{\pi}\mathcal{P}r^{-1/2}, \ A \approx 0.332, & \mathcal{P}r < 3 \times 10^{-4}, \\ \mathcal{P}r^{-0.357+0.022\log\mathcal{P}r}, & 3 \times 10^{-4} \leqslant \mathcal{P}r \leqslant 3, \\ E\,\mathcal{P}r^{-1/3}, \ E \approx 0.982, & \mathcal{P}r > 3. \end{cases} \tag{27}$$

The crossover Prandtl number $\mathcal{P}r^*$ between the asymptotic behaviours, cf the first and the last line of (27), is defined as the intersection point $\mathcal{P}r^* = 0.046$ of the asymptotic approximations. Note that this crossover between the small-$\mathcal{P}r$ behaviour $\delta_\theta/\delta_u \propto \mathcal{P}r^{-1/2}$ and the large-$\mathcal{P}r$ behaviour $\delta_\theta/\delta_u \propto \mathcal{P}r^{-1/3}$ does not happen at a Prandtl number of order 1, but at the more than 20 times smaller value $\mathcal{P}r^* = 0.046$. In this sense, most experiments are conducted in the large $\mathcal{P}r$ regime. However, also note that other definitions of the BL thicknesses lead to other crossover Prandtl numbers.

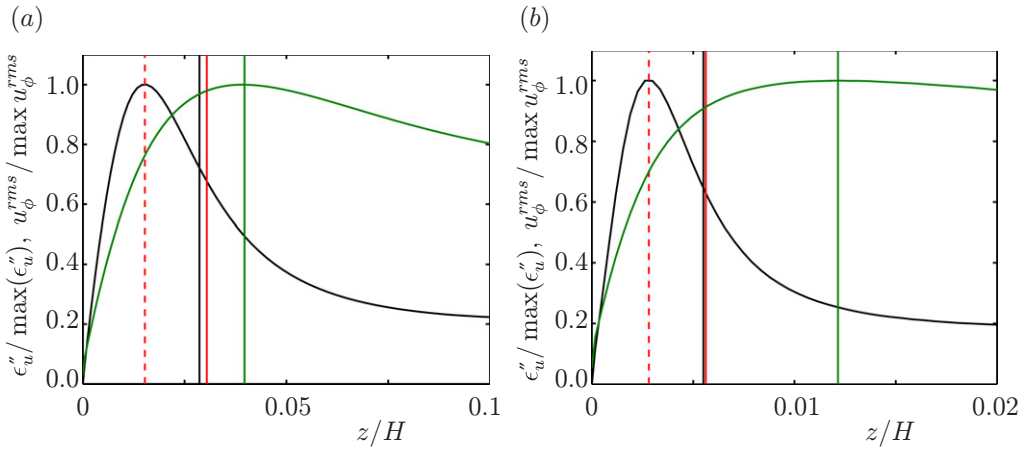

Figure 3. Profiles of ϵ_u'' (29) (black), and the rms velocity fluctuations for the azimuthal velocity component u_ϕ (green) for (*a*) $\mathcal{R}a = 10^8$ and $\mathcal{P}r = 6.4$ and (*b*) $\mathcal{R}a = 2 \times 10^9$ and $\mathcal{P}r = 0.7$. The profiles have been normalized with the respective maxima for clarity. The vertical black lines indicate the velocity BL thickness based on (28). The red dashed and solid lines indicate the heights at which the quantity ϵ_u'' (29) has a maximum and two times this height, respectively. The vertical green line indicates the position of the maximum rms velocity fluctuations.

Finally, we also give the thickness of the kinetic BL in the three regimes, as obtained from (27) and (13), namely

$$\delta_u = \begin{cases} 0.5\mathcal{N}u^{-1}\mathcal{P}r^{1/2}A^{-1}\pi^{-1/2}H, & \mathcal{P}r < 3 \times 10^{-4}, \\ 0.5\mathcal{N}u^{-1}\mathcal{P}r^{0.357-0.022\log\mathcal{P}r}H, & 3 \times 10^{-4} \leqslant \mathcal{P}r \leqslant 3, \\ 0.5\mathcal{N}u^{-1}\mathcal{P}r^{1/3}E^{-1}H, & \mathcal{P}r > 3. \end{cases} \tag{28}$$

We compare this Prandtl–Blasius result (28) for the kinetic BL thickness in terms of $\mathcal{N}u$ and $\mathcal{P}r$ (thus valid if the heat transport is BL dominated) with the estimate given in [21], where the kinetic BL thickness in a cylindrical cell is identified as two times that height at which the averaged quantity

$$\epsilon_u'' := \langle \mathbf{u} \cdot \nabla^2 \mathbf{u} \rangle_{t,\phi,r} \tag{29}$$

has a maximum, because it was empirically found that the maximum of ϵ_u'' is approximately in the middle of the velocity BL. Here, $\mathbf{u}$ is the velocity field and the averaging is over time t, the azimuthal direction ϕ, and over the radial direction $0.1R < r < 0.9R$, with R being the radius of the cylindrical convective cell. The restricted range for the radial direction has been used in order to exclude the singularity region close to the cylinder axis and the region close to the sidewall, where the definition misrepresents the kinetic BL thickness. Figure 3 shows that there is very good agreement between the theoretical Prandtl–Blasius slope BL thickness and that obtained using (29). The figure also shows that the position of the maximum rms velocity fluctuations is not a good indicator of the velocity BL edge; it rather seems to identify the position where the LSC is the strongest.

4. Resolution requirements within the BLs in DNS

We now come to the main point of the paper: what can we learn from the Prandtl–Blasius theory for the required mesh resolution in the BLs of DNS of turbulent RB convection? Obviously, a 'proper' mesh resolution should be used in order to obtain accurate results. In a perfect DNS the local mesh size should be smaller than the local Kolmogorov $\eta_K(\mathbf{x}, t)$ and Batchelor $\eta_B(\mathbf{x}, t)$ scales (see, e.g., [30]), and the resolution in the BLs should be also sufficient (see, e.g., [16, 21, 25, 31, 32]). It indeed has been well established that the Nusselt number is very sensitive to the grid resolution used in the BLs; when DNS is underresolved, the measured Nusselt number is too high [16, 21, 31], [33]–[36]. Hitherto, the standard way to empirically check whether the mesh resolution is sufficient is to try a finer mesh and to make sure that the Nusselt number is not too different. In this way, the minimal number of grid points that is needed in the BL is obtained by trial and error: Grötzbach [31] varied the number of grid points in the BL between 1 and 5 in simulations up to $\mathcal{R}a = 3 \times 10^5$ with $\mathcal{P}r = 0.71$ and found that three grid points in the BLs should be sufficient. Verzicco and Camussi [33] tested this at $\mathcal{R}a = 2 \times 10^7$ and $\mathcal{P}r = 0.7$, and stated that at least five points should be placed in the BLs. Stevens *et al* [21] tested the grid resolution for $\mathcal{R}a = 2 \times 10^6$–$2 \times 10^{11}$ and $\mathcal{P}r = 0.7$. They found that for $\mathcal{R}a = 2 \times 10^9$ the minimum number of nodes in the BLs should be about 10 and that this number increases for increasing $\mathcal{R}a$. Together with the earlier series of papers, the data clearly suggest that indeed there is an increase in required grid points in the BL with increasing Rayleigh number.

However, one must be careful. The empirical determination of the required number of grid points in the BL is not only intensive in computational cost but also difficult. The Nusselt number obtained in the simulations not only depends on the grid resolution in the BLs at the top and bottom plates, but also on the grid resolution in the *bulk* and at the side walls where the thermal plumes pass along [21]. So, obviously, a general theory-based criterion for the required grid resolution in the thermal and kinematic BLs will be helpful for performing future simulations. In this section, we will derive such a universal criterion, harvesting the above results from the Prandtl–Blasius BL theory.

We first define the (local) kinetic energy dissipation rates per mass:

$$\epsilon_u(\mathbf{x}, t) \equiv \frac{\nu}{2} \sum_i \sum_j \left(\frac{\partial u_i(\mathbf{x}, t)}{\partial x_j} + \frac{\partial u_j(\mathbf{x}, t)}{\partial x_i} \right)^2 . \tag{30}$$

Its time and space average for incompressible flow with zero velocity b.c. is $\langle \epsilon_u \rangle_{t,V} = \nu \sum_i \sum_j \langle (\frac{\partial u_i(\mathbf{x},t)}{\partial x_j})^2 \rangle_{t,V}$. It is connected with the Nusselt number through the exact relation

$$\langle \epsilon_u \rangle_{t,V} = \frac{\nu^3}{H^4} (\mathcal{N}u - 1) \mathcal{R}a \mathcal{P}r^{-2}. \tag{31}$$

This follows directly from the momentum equation for RB convection in Boussinesq approximation [37]. Here, $\langle \cdot \rangle_{t,V}$ denotes averaging over the whole volume of the convective cell and over time and (later) $\langle \cdot \rangle_{t,A}$ denotes averaging over any horizontal plane and time.

We start with the well-established criterion that in a perfect DNS simulation the (local) mesh size must not be larger than the (local) Kolmogorov scale [38] $\eta_K(\mathbf{x}, t)$, which is locally defined with the energy dissipation rate of the velocity:

$$\eta_K(\mathbf{x}, t) = \left(\nu^3 / \epsilon_u(\mathbf{x}, t) \right)^{1/4} . \tag{32}$$

η_K is the length scale at which the inertial term $\sim u_r^2/r$ and the viscous term $\sim \nu u_r / r^2$ of the Navier–Stokes equation balance, where $u_r \sim (\epsilon_u r)^{1/3}$ has been assumed for the velocity

difference at scale r. A corresponding length scale η_T follows from the balance of the advection term $\sim u_r T_r/r$ and the thermal diffusion term $\kappa T_r/r^2$ in the advection equation; it is

$$\eta_T(\mathbf{x}, t) = \left(\kappa^3/\epsilon_u(\mathbf{x}, t)\right)^{1/4} = \eta_K(\mathbf{x}, t)\mathcal{P}r^{-3/4}. \tag{33}$$

However, for large $\mathcal{P}r$, the velocity field is smooth at those scales at which the temperature field is still fluctuating. Then the velocity difference $u_r \sim \sqrt{\epsilon_u/\nu}r$ and the advection term and the thermal diffusion term balance at the so-called Batchelor scale [39] η_B, which is defined as

$$\eta_B(\mathbf{x}, t) = \left(\nu\kappa^2/\epsilon_u(\mathbf{x}, t)\right)^{1/4} = \eta_K(\mathbf{x}, t)\mathcal{P}r^{-1/2}. \tag{34}$$

For small $\mathcal{P}r < 1$, obviously $\eta_T > \eta_B > \eta_K$, and for comparison with the grid resolution, the Kolmogorov scale η_K seems to be the most restrictive (i.e. smallest) length scale. In contrast, for large $\mathcal{P}r > 1$, $\eta_T < \eta_B < \eta_K$, and one may argue that η_T is the most restrictive length scale. This indeed may be the case in the Prandtl number regime in which the velocity field can still be described through Kolmogorov scaling $u_r \sim (\epsilon_u r)^{1/3}$, but for even larger $\mathcal{P}r$ the velocity field becomes smooth $u_r \sim \sqrt{\epsilon_u/\nu}\, r$ and then the grid resolution should be compared to the Batchelor scale η_B as the smallest relevant length scale. In the analysis below, for $\mathcal{P}r > 1$ we will restrict ourselves to this limiting case.

We now define the *global* Kolmogorov and Batchelor length scales $\eta_K^{\text{global}} \equiv \frac{\nu^{3/4}}{\langle\epsilon_u\rangle_{t,V}^{1/4}}$ and $\eta_B^{\text{global}} \equiv \frac{\nu^{1/4}\kappa^{1/2}}{\langle\epsilon_u\rangle_{t,V}^{1/4}}$, respectively. Using the exact relation (31), one can find how the global Kolmogorov length η_K^{global} depends on $\mathcal{R}a$, $\mathcal{P}r$ and $\mathcal{N}u$, namely

$$\eta_K^{\text{global}} \equiv \frac{\nu^{3/4}}{\langle\epsilon_u\rangle_{t,V}^{1/4}} = \frac{\mathcal{P}r^{1/2}}{\mathcal{R}a^{1/4}(\mathcal{N}u-1)^{1/4}}H. \tag{35}$$

The admissible global mesh size h^{global} should clearly be smaller than both η_K^{global} and η_B^{global}, which implies that one is on the safe side provided that

$$h^{\text{global}} \leqslant \frac{\mathcal{P}r^{1/2}}{\mathcal{R}a^{1/4}(\mathcal{N}u-1)^{1/4}}H \quad \text{for} \quad \mathcal{P}r \leqslant 1 \tag{36}$$

or with relation (34) between the Kolmogorov and Batchelor length:

$$h^{\text{global}} \leqslant \frac{1}{\mathcal{R}a^{1/4}(\mathcal{N}u-1)^{1/4}}H \quad \text{for} \quad \mathcal{P}r > 1. \tag{37}$$

A similar way to estimate mesh requirements in the bulk was suggested for the first time by Grötzbach [31]. Note that, with these estimates for the required bulk resolution for most times and locations, one is on the safe side, as equation (31) is an estimate for the volume averaged energy dissipation rate, which is localized in the BLs. However, not only the background field but also plumes detaching from the BLs do require an adequate resolution.

To estimate the number of nodes that should be placed in the BLs, we will first estimate the area averaged energy dissipation rate in a horizontal plane in the velocity BL, $\langle\epsilon_u\rangle_{t,A\in\text{BL}}$. Employing equations (17), (14) and (30), one can find a lower bound for this quantity, namely

$$\begin{aligned}\langle\epsilon_u\rangle_{t,A\in\text{BL}} &\geqslant \nu\left\langle\left(\frac{\partial u_x}{\partial z}\right)^2\right\rangle_{t,A} \geqslant \nu\left(\left\langle\frac{\partial u_x}{\partial z}\right\rangle_{t,A}\right)^2 \approx \nu\left(\frac{U}{\delta_u}\right)^2 \\ &= \nu\left(\frac{\nu\mathcal{R}e}{H}\frac{\mathcal{R}e^{1/2}}{aH}\right)^2 = \frac{\nu^3\mathcal{R}e^3}{a^2H^4}.\end{aligned} \tag{38}$$

From equations (31), (38), (18) and (27), it follows a lower bound for the ratio:

$$\frac{\langle \epsilon_u \rangle_{t,A\in \mathrm{BL}}}{\langle \epsilon_u \rangle_{t,V}} \geqslant \frac{\mathcal{P}r^2 \mathcal{R}e^3}{a^2 \mathcal{R}a \mathcal{N}u} = 64 a^4 \mathcal{N}u^5 \frac{\mathcal{P}r^2}{\mathcal{R}a} \left(\frac{\delta_\theta}{\delta_u}\right)^6$$
$$= \begin{cases} 64\pi^3 a^4 A^6 \mathcal{N}u^5 \mathcal{P}r^{-1} \mathcal{R}a^{-1}, & \mathcal{P}r < 3\times 10^{-4}, \\ 64 a^4 \mathcal{N}u^5 \mathcal{P}r^{-0.15+0.132\log \mathcal{P}r} \mathcal{R}a^{-1}, & 3\times 10^{-4} \leqslant \mathcal{P}r \leqslant 3, \\ 64 a^4 E^6 \mathcal{N}u^5 \mathcal{R}a^{-1}, & \mathcal{P}r > 3. \end{cases} \tag{39}$$

For the Kolmogorov length $\eta_{\mathrm{K}}^{\mathrm{BL}}$ in the velocity BL, one can therefore write

$$\eta_{\mathrm{K}}^{\mathrm{BL}} \equiv \left\langle \left(\frac{\nu^3}{\epsilon_u}\right)^{1/4} \right\rangle_{t,A\in \mathrm{BL}} \approx \left(\frac{\langle \epsilon_u \rangle_{t,V}}{\langle \epsilon_u \rangle_{t,A\in \mathrm{BL}}}\right)^{1/4} \eta_{\mathrm{K}}^{\mathrm{global}}. \tag{40}$$

The mesh size h^{BL} in the BL must be smaller than $\eta_{\mathrm{K}}^{\mathrm{BL}}$ and $\eta_{\mathrm{B}}^{\mathrm{BL}}$, i.e. one is on the safe side if

$$h^{\mathrm{BL}} \lesssim \begin{cases} 2^{-3/2} a^{-1} \mathcal{N}u^{-3/2} \mathcal{P}r^{3/4} A^{-3/2} \pi^{-3/4} H, & \mathcal{P}r < 3\times 10^{-4}, \\ 2^{-3/2} a^{-1} \mathcal{N}u^{-3/2} \mathcal{P}r^{0.5355-0.033\log \mathcal{P}r} H, & 3\times 10^{-4} \leqslant \mathcal{P}r \leqslant 1, \\ 2^{-3/2} a^{-1} \mathcal{N}u^{-3/2} \mathcal{P}r^{0.0355-0.033\log \mathcal{P}r} H, & 1 < \mathcal{P}r \leqslant 3, \\ 2^{-3/2} a^{-1} E^{-3/2} \mathcal{N}u^{-3/2} H, & \mathcal{P}r > 3, \end{cases} \tag{41}$$

according to (39), (40), (36) and (37).

From relations (41), (27) and (13), one can estimate the minimum number of nodes of the computational mesh which must be placed in each thermal and kinetic BL close to the plates. We find that this minimum number of nodes in the thermal BLs is

$$N_{\mathrm{th.BL}} \equiv \frac{\delta_\theta}{h^{\mathrm{BL}}}$$
$$\gtrsim \begin{cases} \sqrt{2} a \mathcal{N}u^{1/2} \mathcal{P}r^{-3/4} A^{3/2} \pi^{3/4}, & \mathcal{P}r < 3\times 10^{-4}, \\ \sqrt{2} a \mathcal{N}u^{1/2} \mathcal{P}r^{-0.5355+0.033\log \mathcal{P}r}, & 3\times 10^{-4} \leqslant \mathcal{P}r \leqslant 1, \\ \sqrt{2} a \mathcal{N}u^{1/2} \mathcal{P}r^{-0.0355+0.033\log \mathcal{P}r}, & 1 < \mathcal{P}r \leqslant 3, \\ \sqrt{2} a \mathcal{N}u^{1/2} E^{3/2}, & \mathcal{P}r > 3, \end{cases} \tag{42}$$

while the minimum number of nodes in the kinetic BLs is

$$N_{\mathrm{v.BL}} \equiv \frac{\delta_u}{h^{\mathrm{BL}}} = \frac{\delta_u}{\delta_\theta} \frac{\delta_\theta}{h^{\mathrm{BL}}}$$
$$\gtrsim \begin{cases} \sqrt{2} a \mathcal{N}u^{1/2} \mathcal{P}r^{-1/4} A^{1/2} \pi^{1/4}, & \mathcal{P}r < 3\times 10^{-4}, \\ \sqrt{2} a \mathcal{N}u^{1/2} \mathcal{P}r^{-0.1785+0.011\log \mathcal{P}r}, & 3\times 10^{-4} \leqslant \mathcal{P}r \leqslant 1, \\ \sqrt{2} a \mathcal{N}u^{1/2} \mathcal{P}r^{0.3215+0.011\log \mathcal{P}r}, & 1 < \mathcal{P}r \leqslant 3, \\ \sqrt{2} a \mathcal{N}u^{1/2} \mathcal{P}r^{1/3} E^{1/2}, & \mathcal{P}r > 3. \end{cases} \tag{43}$$

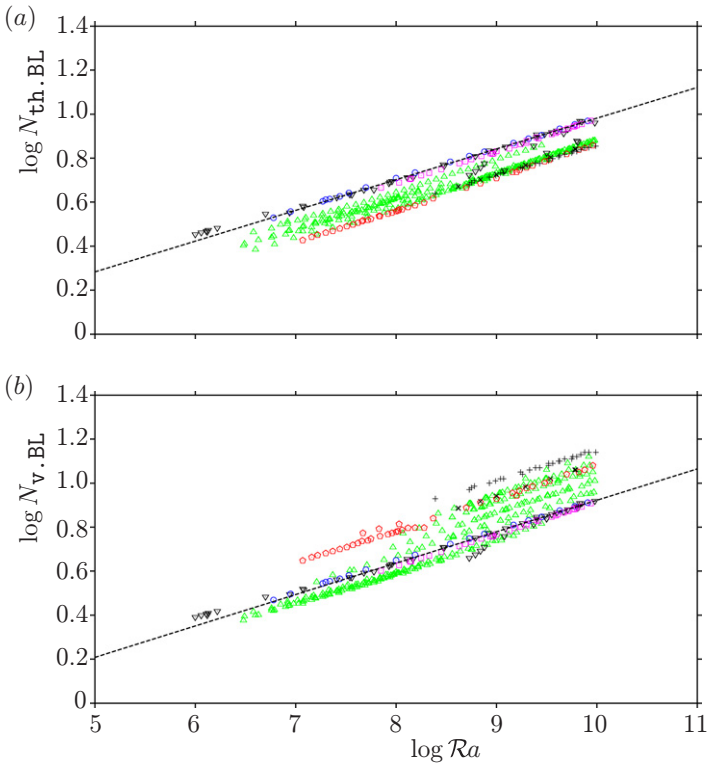

Figure 4. Minimum number of BL nodes necessary in DNS of BL dominated, moderately high RB convection. (a) $N_{\mathrm{th.BL}}$ (42) in the thermal BLs and (b) $N_{\mathrm{v.BL}}$ (43) in the kinetic BLs, required to simulate the experimentally investigated cases, [40] (lilac squares, $\mathcal{P}r = 0.67$), [41] (black triangles, $0.60 \leqslant \mathcal{P}r \leqslant 7.00$), [42] (blue circles, $0.68 \leqslant \mathcal{P}r \leqslant 5.92$), [43] (green triangles, $0.73 \leqslant \mathcal{P}r \leqslant 6.00$), [44] (red pentagons, $3.76 \leqslant \mathcal{P}r \leqslant 5.54$), [45] (black crosses, $\mathcal{P}r = 4.2$) and [46] (black pluses, $\mathcal{P}r = 7.0$). Dashed lines are fits to the quasi-data (measured values introduced into equations (42) and (43)), with precision $\mathrm{O}(10^{-4})$; rounding the respective numbers to their upper bounds gives (a) $N_{\mathrm{th.BL}} \approx 0.35\mathcal{R}a^{0.15}$ (44) and (b) $N_{\mathrm{v.BL}} \approx 0.31\mathcal{R}a^{0.15}$ (45) for the quasi-data in the ranges $10^6 \leqslant \mathcal{R}a \leqslant 10^{10}$ and $0.67 \leqslant \mathcal{P}r \leqslant 0.73$.

The number of nodes in the thermal BL looks very restrictive for very low $\mathcal{P}r$. However, one should realize that for very low $\mathcal{P}r$ the thermal BL also becomes much thicker than the velocity BL. Hence, the criterion for the number of nodes in the thermal BLs determines the ideal distribution of nodes above the viscous BL. For very high $\mathcal{P}r$ the kinetic BL becomes much thicker than the thermal BL and hence the restriction for the velocity BL determines the ideal distribution of nodes above the thermal BL. Note that for large $\mathcal{P}r$, equation (42) suggests that the number of grid points in the thermal BL becomes independent of $\mathcal{P}r$ (for fixed $\mathcal{N}u$). Indeed, as the velocity field is smooth anyhow, with increasing $\mathcal{P}r$ no extra grid points are necessary in the thermal BL.

In figure 4, we show the minimum number of nodes $N_{\mathrm{th.BL}}$ and $N_{\mathrm{v.BL}}$, respectively, necessary to simulate the cases that have been investigated experimentally so far, for different $\mathcal{R}a$ and $\mathcal{P}r$. The data points are generated by introducing the experimental values of $\mathcal{R}a$ and $\mathcal{P}r$

and the (measured) corresponding $\mathcal{N}u$ into formulae (42) and (43). Based on these quasi-data points, one can give, e.g., the following fits for the minimum number of nodes within the BLs for the case of $\mathcal{P}r \approx 0.7$:

$$N_{\mathrm{th.BL}} \approx 0.35\mathcal{R}a^{0.15}, \quad 10^6 \leqslant \mathcal{R}a \leqslant 10^{10}, \tag{44}$$

$$N_{\mathrm{v.BL}} \approx 0.31\mathcal{R}a^{0.15}, \quad 10^6 \leqslant \mathcal{R}a \leqslant 10^{10}. \tag{45}$$

Note that the numerical pre-factors in these estimates significantly depend on the Prandtl number and on the empirically determined [5] value of a (cf equation (15)). The minimum number of nodes for other values of $\mathcal{P}r$ can be calculated directly using relations (42) and (43). Apparently, the scaling exponent depends much less on $\mathcal{P}r$. All these estimates only give lower bounds on the required number of nodes in the BLs.

As discussed at the beginning of this section, previous studies by Grötzbach [31], Verzicco and Camussi [33] and Stevens *et al* [21] found an increasing number of nodes that should be placed in the thermal and kinetic BLs. The theoretical results thus confirm all the above studies, because the increasing number of nodes was due to the increasing $\mathcal{R}a$ number at which the tests were performed. To be more specific, according to the estimates (44) and (45) for $\mathcal{P}r = 0.7$, the minimum number of nodes that should be placed in the thermal and kinetic BLs is $N \approx 2.3$ for $\mathcal{R}a = 3 \times 10^5$, $N \approx 4.4$ for $\mathcal{R}a = 2 \times 10^7$ and $N \approx 8.7$ for $\mathcal{R}a = 2 \times 10^9$. The empirically found values at the respective $\mathcal{R}a$ with $\mathcal{P}r \approx 0.7$ are 3 for $\mathcal{R}a = 3 \times 10^5$, 5 for $\mathcal{R}a = 2 \times 10^7$ and 10 for $\mathcal{R}a = 2 \times 10^9$. Thus there is very good agreement between the theoretical results and the empirically obtained values, especially if one considers the difficulties involved in determining these values empirically, and the empirical value for the constant a (15) that is used in the theoretical estimates. We want to emphasize that not only the BLs close to the plates, but also the kinetic BLs close to the vertical walls, must be well resolved.

To sum up, the mesh resolution should be analysed *a priori* using the resolution requirements in the bulk (36), (37) *and* in the BLs (42), (43). Having conducted the DNS, the Kolmogorov and Batchelor scale should be checked *a posteriori*, to make sure that the mesh size was indeed small enough (as it has been done, for example, in [19, 20]).

5. Conclusion

In summary, we used the laminar Prandtl–Blasius BL theory to determine the relative thicknesses of the thermal and kinetic BLs as functions of $\mathcal{P}r$ (27).

We found that neither the position of the maximum rms velocity fluctuations nor the position of the horizontal velocity maximum reflects the slope velocity BL thickness, although many studies use these as criteria to determine the BL thickness. In contrast to them, the algorithm by Stevens *et al* [21] agrees very well with the theoretical estimate of the kinetic slope BL thickness.

We used the results obtained from the Prandtl–Blasius BL theory to derive a lower bound on the minimum number of nodes that should be placed in the thermal and kinetic BLs close to the plates. We found that this minimum number of nodes increases no slower than $\sim\mathcal{R}a^{0.15}$ with increasing $\mathcal{R}a$. This result is in excellent agreement with results from several numerical studies over recent decades, in which this minimum number of nodes was determined empirically. Hence, the derived estimates can be used as a guideline for future DNS.

Acknowledgments

OS thanks Professor Dr-Ing. C Wagner and Deutsche Forschungsgemeinschaft (DFG) for support of this work under grant no. WA1510/9. The Twente part of the work was supported by the Foundation for Fundamental Research on Matter (FOM), sponsored by NWO.

References

[1] Ahlers G, Grossmann S and Lohse D 2009 *Rev. Mod. Phys.* **81** 503
[2] Lohse D and Xia K Q 2010 *Annu. Rev. Fluid Mech.* **42** 335–64
[3] Grossmann S and Lohse D 2000 *J. Fluid. Mech.* **407** 27–56
[4] Grossmann S and Lohse D 2001 *Phys. Rev. Lett.* **86** 3316–9
[5] Grossmann S and Lohse D 2002 *Phys. Rev.* E **66** 016305
[6] Grossmann S and Lohse D 2004 *Phys. Fluids* **16** 4462–72
[7] Landau L D and Lifshitz E M 1987 *Fluid Mechanics* (Oxford: Pergamon)
[8] Sun C, Cheung Y H and Xia K Q 2008 *J. Fluid Mech.* **605** 79–113
[9] Prandtl L 1905 über Flüssigkeitsbewegung bei sehr kleiner Reibung *Verhandlungen des III. Int. Math. Kongr.* (*Heidelberg, 1904*) (Leipzig: Teubner) pp 484–91
[10] Blasius H 1908 *Z. Math. Phys.* **56** 1–37
[11] Pohlhausen K 1921 *Z. Angew. Math. Mech.* **1** 252–68
[12] Meksyn D 1961 *New Methods in Laminar Boundary Layer Theory* (Oxford: Pergamon)
[13] Schlichting H 1979 *Boundary Layer Theory* 7th edn (New York: McGraw-Hill)
[14] Zhou Q and Xia K Q 2010 *Phys. Rev. Lett.* **104** 104301
[15] Zhou Q, Stevens R J A M, Sugiyama K, Grossmann S, Lohse D and Xia K Q 2010 *J. Fluid Mech.* at press arXiv:1002.1339
[16] Kerr R 1996 *J. Fluid Mech.* **310** 139–79
[17] Verzicco R and Camussi R 1997 *Phys. Fluids* **9** 1287–95
[18] Kerr R and Herring J R 2000 *J. Fluid Mech.* **419** 325–44
[19] Shishkina O and Wagner C 2007 *Phys. Fluids* **19** 085107
[20] Shishkina O and Wagner C 2008 *J. Fluid Mech.* **599** 383–404
[21] Stevens R J A M, Verzicco R and Lohse D 2010 *J. Fluid Mech.* **643** 495–507
[22] Calzavarini E, Lohse D, Toschi F and Tripiccione R 2005 *Phys. Fluids* **17** 055107
[23] Ahlers G, Brown E, Fontenele Araujo F, Funfschilling D, Grossmann S and Lohse D 2006 *J. Fluid Mech.* **569** 409–45
[24] Stevens R J A M, Clercx H J H and Lohse D 2010 *New J. Phys.* **12** 075005
[25] Shishkina O and Thess A 2009 *J. Fluid Mech.* **633** 449–60
[26] Qiu X L and Tong P 2001 *Phys. Rev. Lett.* **87** 094501
[27] DeLuca E E, Werne J, Rosner R and Cattaneo F 1990 *Phys. Rev. Lett.* **64** 2370–3
[28] Schmalzl J, Breuer M, Wessling S and Hansen U 2004 *Europhys. Lett.* **67** 390–6
[29] Sugiyama K, Calzavarini E, Grossmann S and Lohse D 2009 *J. Fluid Mech.* **637** 105–35
[30] Monin A S and Yaglom A M 1975 *Statistical Fluid Mechanics* (Cambridge, MA: MIT)
[31] Grötzbach G 1983 *J. Compd. Phys.* **49** 241–64
[32] Shishkina O, Shishkin A and Wagner C 2009 *J. Comput. Appl. Math.* **226** 336–44
[33] Verzicco R and Camussi R 2003 *J. Fluid Mech.* **477** 19–49
[34] Amati G, Koal K, Massaioli F, Sreenivasan K R and Verzicco R 2005 *Phys. Fluids* **17** 121701
[35] Verzicco R and Sreenivasan K R 2008 *J. Fluid Mech.* **595** 203–19
[36] Verdoold J, van Reeuwijk M, Tummers M J, Jonker H J J and Hanjalić K 2008 *Phys. Rev.* E **77** 016303
[37] Siggia E D 1994 *Annu. Rev. Fluid Mech.* **26** 137–68
[38] Kolmogorov A N 1941 *Dokl. Akad. Nauk. SSSR* **30** 299–303

[39] Batchelor G K 1959 *J. Fluid Mech.* **5** 113–33
[40] Ahlers G, Bodenschatz E, Funfschilling D and Hogg J 2009 *J. Fluid Mech.* **641** 157–67
[41] Chavanne X, Chilla F, Chabaud B, Castaing B and Hebral B 2001 *Phys. Fluids* **13** 1300–20
[42] Niemela J and Sreenivasan K R 2003 *J. Fluid Mech.* **481** 355–84
[43] Roche P E, Castaing B, Chabaud B and Hebral B 2004 *J. Low Temp. Phys.* **134** 1011–42
[44] Sun C, Ren L Y, Song H and Xia K Q 2005 *J. Fluid Mech.* **542** 165–74
[45] Xia K Q, Lam S and Zhou S Q 2002 *Phys. Rev. Lett.* **88** 064501
[46] Qiu X L and Xia K Q 1998 *Phys. Rev.* E **58** 486–91